Dr. Morishita is a member of the Institute of Electronics and Communication Engineers of Japan and the Society of Instrument and Control Engineers of Japan.

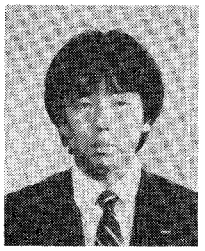

Hiroshi Ikeda was born in Kobe, Japan, on October 28, 1957. He received the B.E. degree in electrical communication engineering from Osaka University, Osaka, Japan, in 1981. He worked there on research in the areas of electromagnetic theory and optical waveguides.

He is presently with Asahi Broadcasting Company, Osaka, Japan.

Nobuaki Kumagai (M'59–SM'71–F'81) was born in Ryojun, Japan, on May 19, 1929. He received the B. Eng. and D. Eng. degrees from Osaka University, Osaka, Japan, in 1953 and 1959, respectively.

From 1956 to 1960 he was an Assistant Professor of Communication Engineering Department at Osaka University, Osaka, Japan. From 1958 through 1960 he was a Visiting Senior Research Fellow at the Electronics Research Laboratory of the University of California, Berkeley, on leave of absence from Osaka University. From 1960 to 1970 he was an Associate Professor, and has been a Professor of Communication Engineering at Osaka University since 1971. He served as a Department Chairman in the periods of 1972-1973 and 1977-1978. Since 1980 he was installed as the Dean of Student Affairs of Osaka University, serving concurrently as Professor of Communication Engineering.

His fields of interest are theory of electromagnetic fields and waves, microwaves, millimeter-waves, acoustic-waves engineering, optical fibers, optical integrated circuits and devices, lasers and their applications. He published more than one hundred technical papers in established journals on these topics. He is the co-author of *Microwave Circuits* (OHM-sha, Tokyo, 1963) and *Introduction to Relativistic Electromagnetic Field Theory* (Corona Publishing Co., Tokyo, 1971). From 1979 to 1981 he was President of the Microwave Theory and Techniques Society of the Institute of Electronics and Communication Engineers of Japan.

Dr. Kumagai is a member of the Institute of Electronics and Communication Engineers of Japan, the Institute of Electrical Engineers of Japan, and the Laser Society of Japan.

Slow Wave Gyrotron Amplifier with a Dielectric Center Rod

JOON Y. CHOE, HAN S. UHM, AND SAEYOUNG AHN, MEMBER, IEEE

Abstract—**The broad-band capability of the gyrotron amplifier with a dielectric center rod is investigated. The dispersion relation for the TE mode perturbation is obtained, and the system parameters for the optimum bandwidth are obtained for a small axial velocity spread. It is found that the dielectric center rod extends the frequency range of the intermediate wavelength mode (IWM), and reduces the contribution of the troublesome short wavelength mode (SWM). The bandwidth and the gain due to the IWM for the center rod geometry are superior to those for the wall clad dielectric gyrotron.**

I. Introduction

RECENTLY there have been numerous studies [1]–[6] on the dielectric loaded gyrotron for a wide-band application. It has been found [2], [4], [6] that there exist three unstable modes characterized by their axial phase velocities (v_{ph}); the long wavelength mode (LWM, $v_{ph} > c$), the intermediate wavelength mode (IWM, $c > v_{ph} > c\epsilon^{-1/2}$), and the short wavelength mode (SWM, $v_{ph} < c$). Here ϵ and c are the dielectric constant and the velocity of light. For a small axial velocity spread ($\lesssim 1$ percent), two slow wave modes (IWM and SWM) yield very promising bandwidth capability [2], especially when two modes are mixed by placing the beam close to the axis [4], [6]. However, the nature of the SWM [2], [4], whose perturbed fields are almost entirely supported by the electron beam, not by the waveguide, raises the difficulties related to the excitation and collection of the electromagnetic waves [2], [4]. One possible solution to this difficulty is to utilize the dielectric material as a center rod [7], rather than as an outside wall loading [1]–[5]. By using dielectric material as a center rod, it will be shown that the frequency range of the IWM is extended, while the contribution of the troublesome SWM is minimized.

Manuscript received August 18, 1981; revised October 28, 1981. This research was supported in part by an Independent Research Fund at the Naval Surface Weapons Center, and in part by the Office of Naval Research.

J. Y. Choe and H. S. Uhm are with the Naval Surface Weapons Center, White Oak, Silver Spring, MD 20910.

S. Ahn is with the Naval Research Laboratory, Washington, D.C. 20375.

The dispersion relation for the gyrotron with a dielectric center rod has been derived by the authors [7] for general azimuthal (θ) mode numbers (i.e., $l \neq 0$). In this paper, we will perform a detailed numerical investigation of this dispersion equation for a broad range of the physical parameters, and compare the results with those of the gyrotron with the outer dielectric loading [2], [4], [6]. For simplicity, the present investigation is limited to the azimuthally symmetric (i.e., $l = 0$), transverse electric (TE) perturbations. Moreover, in view of the relative insensitivity of the fast wave mode (LWM) to the system parameters [2], [6], [7], we will devote our attention only to the slow wave modes (IWM and SWM). A complete parametric optimization process for wide bandwidth will be carried out, assuming that the axial velocity spread of the beam electrons is small ($=1$ percent) [6]. The optimization is carried out in the spirit of maximizing the contribution of the IWM to the bandwidth, and minimizing that of the SWM. In addition, the perturbed field profiles are examined in order to distinguish the IWM and SWM.

The slow wave modes (IWM and SWM) for the center rod gyrotron do not compete with each other in their contribution to the instability as much as for the wall clad configuration. This cooperative nature of the IWM and the SWM results in an extended IWM region compared to the wall clad geometry. That is, the SWM begins to contribute significantly at higher frequency than it does in the outside loaded gyrotron. On the other hand, it will be shown that the bandwidth itself for the center rod configuration is approximately as wide as that for the wall clad one (see Section III). Thus, by putting the dielectric rod at the center, we are able to maintain about the same wide-band capability, while eliminating some of the difficulties associated with the SWM.

A brief review of the derivation procedure for the dispersion relation will be given in Section II. The expressions for the perturbed fields are also given in Section II for later use. The optimization for the wide bandwidth with 1 percent of the axial velocity spread is carried out in Section III. The physical parameters to be optimized are the thickness ratio of the dielectric center rod (R_d/R_c), the dielectric constant (ϵ), the conducting wall radius (R_c), and the beam center location (R_0). In Section IV, the perturbed field profiles are investigated in order to examine the individual contribution of the IWM and the SWM to the bandwidth. Especially, we compare these field profiles with those of the wall clad configuration. The summary of the comparison is given in the Conclusion.

II. Dispersion Relation

The cross section of the gyrotron with a dielectric center rod is shown in Fig. 1. A cylindrical dielectric (ϵ) rod of radius R_d is located concentrically with the conducting wall of radius R_c. The hollow electron beam passes through the space between the dielectric center rod and the conducting wall. The individual electrons undergo the cyclotron motion with Larmor radii r_L about the beam center location

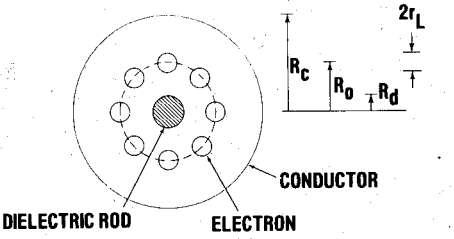

Fig. 1. Cross section of a gyrotron with a dielectric center rod.

R_0, under the influence of a constant applied axial magnetic field B_0. In addition, the electron beam moves downstream with the axial velocity. The cylindrical coordinates (r, θ, z) are employed.

The dispersion relation is derived within the framework of the Vlasov–Maxwell equations for the fields $\boldsymbol{E}(\boldsymbol{x}, t)$ and $\boldsymbol{B}(\boldsymbol{x}, t)$, and for the beam electron distribution function $f(\boldsymbol{x}, \boldsymbol{p}, t)$. Here $\boldsymbol{x}$, $\boldsymbol{p}$, and t refer to the spatial, momentum, and the time coordinates. Further, any quantity ψ is linearized according to

$$\psi(\boldsymbol{x}, t) = \psi_0(r) + \psi_1(r) \exp[i(kz - \omega t)] \tag{1}$$

with the equilibrium quantity ψ_0 and the small Fourier decomposed perturbation ψ_1. Note that we limit our attention to the azimuthally symmetric perturbation ($\partial/\partial\theta = 0$) with the frequency ω and the axial wavenumber k. Moreover, we will consider the transverse electric (TE, $E_{z1} = 0$) perturbation only. It is assumed that the beam is tenuous, and the beam thickness is small [1], [2], [4], [6], [7]. In order to examine the effect of the axial velocity spread, the equilibrium distribution function f_0 is assumed to be Lorentzian [2], [4], [6], [7] in the axial momentum p_z, that is

$$f_0 \propto \hat{p}_z \Delta \left[(p_z - \hat{p}_z)^2 + \hat{p}_z^2 \Delta^2 \right]^{-1}. \tag{2}$$

Here $\hat{p}_z$ is the average axial linear momentum and Δ is the axial momentum spread ratio. The beam is further assumed to be monoenergetic with energy γmc^2, and the average transverse (axial) velocity is given by $c\beta_\perp (c\beta_z)$.

Since the details of the procedures in obtaining the dispersion relation are given in [7], here we present only the outline. Making use of the thin beam approximation and the boundary conditions on the azimuthal electric field $E_{\theta 1}$ at $r = 0$, R_d, R_0, and R_c, within a normalizing factor we obtain the perturbed fields $\boldsymbol{E}_1$ and $\boldsymbol{B}_1$

$$E_{\theta 1} = \begin{cases} J_1(y), & 0 \leq r \leq R_d \\ -\dfrac{\pi}{2}\left[A_{JN} J_1(x) - A_{JJ} N_1(x)\right], & R_d \leq r \lesssim R_0 \\ -\dfrac{\pi}{2}\dfrac{B_2}{B_3}\left[N_1(x_c) J_1(x) - J_1(x_c) N_1(x)\right], & R_0 \lesssim r \leq R_c \end{cases} \tag{3}$$

$$B_{r1} = -\frac{ck}{\omega} E_{\theta 1}, B_{z1} = -\frac{ic}{\omega}\frac{1}{r}\frac{\partial}{\partial r}(rE_{\theta 1}). \tag{4}$$

The jump condition on B_{z1} across the beam furnishes the

desired dispersion relation. Namely

$$\frac{B_N}{B_D} = -\frac{\nu\beta_\perp^2 c^2}{2\gamma R_0^2\left[\omega - \omega_B + i|k|c\beta_z\gamma\Delta/\gamma_z^3\right]^2} \tag{5}$$

with the wave admittance [1], [2], [4], [6], [7] B_N/B_D given by

$$\begin{aligned} B_N &= 2B_1, B_D = -\pi x_0^2 B_2 B_3 \\ B_1 &= J_1(x_c)A_{JN} - N_1(x_c)A_{JJ} \\ B_2 &= J_1(x_0)A_{JN} - N_1(x_0)A_{JJ} \\ B_3 &= J_1(x_0)N_1(x_c) - N_1(x_0)J_1(x_c) \end{aligned} \tag{6}$$

$$\begin{Bmatrix} A_{JJ} \\ A_{JN} \end{Bmatrix} \equiv y_d J_0(y_d) \begin{Bmatrix} J_1(x_d) \\ N_1(x_d) \end{Bmatrix} - x_d \begin{Bmatrix} J_0(x_d) \\ N_0(x_d) \end{Bmatrix} J_1(y_d).$$

The arguments of the Bessel functions of first (J) and second (N) kind are

$$\begin{Bmatrix} y^2 \\ y_d^2 \end{Bmatrix} \equiv \left(\frac{\omega^2}{c^2}\epsilon - k^2\right) \begin{Bmatrix} r^2 \\ R_d^2 \end{Bmatrix}$$

$$\begin{Bmatrix} x^2 \\ x_d^2 \\ x_0^2 \\ x_c^2 \end{Bmatrix} \equiv \left(\frac{\omega^2}{c^2} - k^2\right) \begin{Bmatrix} r^2 \\ R_d^2 \\ R_0^2 \\ R_c^2 \end{Bmatrix}. \tag{7}$$

In (5), the Doppler-shifted beam mode ω_B is defined by

$$\omega_B \equiv kc\beta_z + \omega_c/\gamma. \tag{8}$$

The Budker parameter (ν) is given by $\nu \equiv Ne^2/mc^2$, $\omega_c \equiv eB_0/mc$ is the nonrelativistic electron cyclotron frequency, and $\gamma_z \equiv (1-\beta_z^2)^{-1/2}$ is the axial mass factor. Here N is the total number of electrons per unit axial length, and $(-e)$ and m are the charge and the rest mass of the electron. It is easy to show that the dispersion relation in [7] yields the identical result (5) in the limit of $l = 0$.

The dispersion relation (5) is numerically solved for the axial wavenumber k in terms of the frequency ω, when other beam and geometric parameters (ν, $\beta_\perp$, β_z, Δ, R_0, ϵ, R_c, R_d) are given. If the solution k is complex, the mode is unstable, and the gain is given by the negative value of the imaginary part of k (i.e., $-k_i \equiv -\mathrm{Im}(k)$, when $k_i < 0$). The characteristics of the unstable modes thus obtained are very similar to those with the wall clad dielectric gyrotron [2]. The TE perturbation exhibits three unstable modes; one fast wave mode (LWM) and two coexisting slow wave modes (IWM and SWM) separated by a stable band near the $\omega = ck$ line. Both the LWM and IWM originate from the unstable coupling of the beam mode ω_B ((8)) and the beam-free waveguide mode ω_G (the solution of $B_N = 0$ in (5) and (6)). On the other hand, the SWM is driven by a quasi-static magnetic dipole moment instability [6], [8], characterized by highly localized perturbed fields near the beam location ([2], [4], [6], and see Section IV). As in the case of the wall clad geometry, the reduction in the gain due to the axial velocity spread (Δ in (2)) is the least for the LWM, moderate for the IWM, and the largest for the SWM. On the other hand, the bandwidth at small axial velocity spread ($\Delta \lesssim 1$ percent) is the broadest for the SWM, intermediate for the IWM, and the narrowest for the LWM. Since our objective is to achieve wide bandwidth, we will concentrate only on the slow waves (IWM and SWM) in the remainder of this paper. In view of the difficulties associated with the SWM (excitation and collection of the electromagnetic waves), we attempt to find the parameter conditions where the IWM shows a wide bandwidth, over which the SWM is substantially suppressed.

In light of our intention to minimize the SWM contribution, there are several ways to distinguish the integrated two slow waves (IWM and SWM). One method is to utilize the different vulnerability of their gains on the velocity spread (Δ). Although we choose $\Delta = 1$ percent for our investigation, we therefore examine the gain for $\Delta = 3$ percent as well. If the gain is substantial for both $\Delta = 1$ percent and 3 percent, we identify this instability due to the IWM. On the other hand, if the gain is greatly reduced for $\Delta = 3$ percent, we label them as the SWM. The other method to distinguish the two modes is to examine the perturbed field profile. If the field profile is very similar to that of the beam-free waveguide, then the instability is due to the beam-waveguide coupling IWM. If, however, the field profile is highly localized near the beam location, we attribute the gain to the SWM. The former method is used in Section III and the latter in Section IV.

III. Parametric Optimization

In this section we will obtain the optimized physical parameters for the wide-band gyrotron amplifier; the thickness ratio of the dielectric center rod (R_d/R_c), the conducting wall radius (R_c), the dielectric constant (ϵ), and the beam location (R_0). We again emphasize that the optimization is for the bandwidth due to the IWM, minimizing the contribution of the troublesome SWM. In the remainder of this paper, we assume the following beam parameters:

$$\beta_\perp = 0.4 \quad \beta_z = 0.2 \quad \nu = 0.002 \tag{9}$$

corresponding to 60.3 kV of the anode voltage and 6.8 A of total axial current. For future reference, we also define

$$R_c^0 \equiv 4.197\, c/\omega_c. \tag{10}$$

It can be shown that R_c^0 is the optimized wall radius when the dielectric is absent [2], [4], [6]. The axial velocity spread (Δ) of the beam is assumed to be small ($\Delta = 1$ percent). However, in order to examine the contribution of the SWM (to be minimized), the case for $\Delta = 3$ percent is also examined for reference.

Since the IWM results from the coupling of the beam mode ω_B ((8)) and the beam-free waveguide mode ω_G ($B_N = 0$ in (6)), much information on the IWM can be extracted by examining the two modes, $\omega_B(\beta_\perp, B_z, \omega_c)$ and $\omega_G(R_d, R_c, \epsilon)$. In Fig. 2, a schematic diagram of the mode characteristics is given in the space of the conducting wall radius (R_c) and the dielectric constant (ϵ). The dispersion

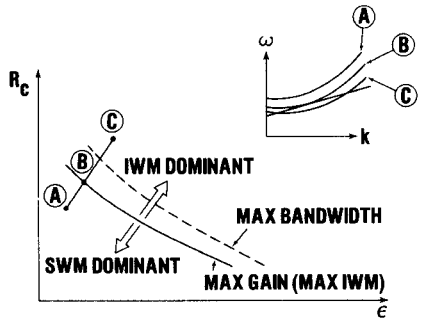

Fig. 2. Schematic diagram of the mode characteristics in the space of the conducting wall radius (R_c) and the dielectric constant (ϵ). The dispersion curves for the parameters represented by A, B, and C are shown in the upper corner. The maximum bandwidth curve (broken) is located above the maximum gain curve in $R_c - \epsilon$ space.

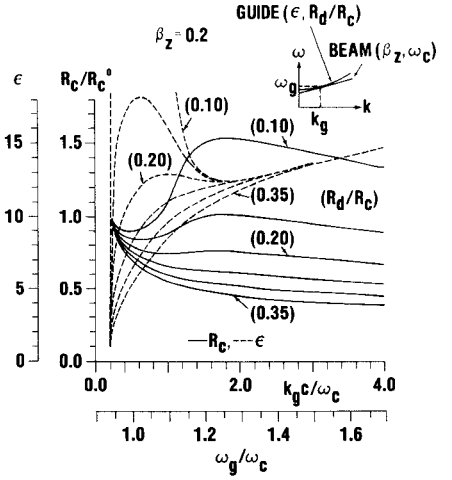

Fig. 3. Grazing conditions on the conducting wall radius (R_c,—) and the dielectric constant (ϵ,---). The values of R_c and ϵ that make the beam mode graze the waveguide mode (upper corner) are shown for several values of the thickness parameter (R_d/R_c).

curves for the parameters denoted by A, B, and C are schematically shown in the upper corner. When the beam mode ω_B (the straight line in the upper corner diagram) grazes the waveguide mode ω_G (case B), the IWM gain is maximum. For the parameters *above* the maximum gain curve (solid curve in Fig. 2), ω_B intersects ω_G more than one time (case C), and for the parameters *below* the maximum gain line, ω_B does not intersect ω_G at all (case A). Since the IWM gain is maximum at the $\omega_B - \omega_G$ intersecting points, it is obvious that the SWM is dominant when the parameters (R_c and ϵ) are well below the maximum IWM gain line, while at near and above it, the IWM is dominant as shown. Above the maximum IWM gain line, where ω_B intersects ω_G more than one time, the gain yields multiple maxima in ω-space with a valley in between. Therefore, we expect that the maximum bandwidth line (broken) is located slightly above the maximum gain line (solid). Along the maximum bandwidth line, the gain at the valley in $k_i - \omega$ diagram is just high enough so that the bandwidth covers both maxima, to yield broadest bandwidth. As one moves further above the maximum bandwidth line, the valley of $k_i - \omega$ diagram is too deep to extend the bandwidth to both maxima, thereby abruptly decreasing the bandwidth. All these arguments will be later confirmed in the numerical investigations.

After seeing that the beam-waveguide grazing condition (case B in Fig. 2) plays an important role in predicting both the gain and the bandwidth of the IWM, we now proceed to find the grazing conditions for the beam parameters given in (9). The results are summarized in Fig. 3, where the values of the wall radius (R_c, solid lines) and the dielectric constant (ϵ, broken lines) that make the beam mode graze the waveguide mode (upper corner) are plotted. The thickness ratio of the dielectric rod (R_d/R_c) varies from 0.10 to 0.35 with 0.05 increment. The results in Fig. 3 are similar to those for the wall clad configuration [2, fig. 7]. However, there are several noteworthy differences. In general, the center rod configuration yields larger wall radius, and smaller dielectric constant compared to the wall clad gyrotron. For example, for the same thickness ratio ($R_d/R_c = 0.20$ for the center rod, $R_w/R_c = 0.80$ for the wall clad, where R_w is the inner radius of the dielectric material), $R_c/R_c^0 = 0.7 \sim 0.8$, $\epsilon = 12 \sim 13$ in the IWM frequency range for the center rod, and $R_c/R_c^0 = 0.5 \sim 0.6$, $\epsilon = 13 \sim 15$ for the wall clad case. The larger wall radius for the center rod configuration may be an advantage when the operating frequency is very high. We note from Fig. 3 that for the thickness ratio $R_d/R_c = 0.20$, the grazing R_c or ϵ remains relatively unchanged over the IWM frequency range (i.e., $\omega/\omega_c > 1.1$). That is, at this dielectric configuration ($R_d/R_c = 0.20$), the beam mode grazes or nearly grazes the waveguide mode for a broad range of the frequency in the IWM region, thereby resulting in a wide bandwidth. We therefore conclude that the optimized rod thickness ratio is given by $R_d/R_c = 0.20$. However, we also note that the value of ϵ or R_c, although relatively flat, varies more sensitively than that for the wall clad case [2]. This enhanced sensitivity aids the center rod gyrotron in achieving wider bandwidth, although at smaller gain, compared to the wall clad case. This will be confirmed later in the numerical investigations.

The relative sensitivity of the gain to the variation of R_c or ϵ for the center rod configuration necessitates additional optimization investigations on R_c and ϵ. These are illustrated in Figs. 4 and 5. With the beam parameters (9) and the optimized rod thickness ratio $R_d/R_c = 0.20$, the linear gain ($-k_i$) is numerically obtained from the dispersion relation (5), as a function of the frequency (ω) for various values of the wall radius R_c and the dielectric constant ϵ. The maximum value of the gain ($-k_i^{\max}$) in the $k_i - \omega$ diagram is shown in Fig. 4, which determines the maximum gain curve in the $R_c - \epsilon$ space in Fig. 2. Although the chosen velocity spread (Δ) is 1 percent, those for $\Delta = 3$ percent are also shown as a reference. For $\Delta = 1$ percent, the plot of k_i versus ω yields multiple maxima for ϵ higher than a certain value, denoted in the figure with dotted lines. This multiple maxima phenomenon is expected from the considerations in Fig. 2, corresponding to the case C. On the other hand, for $\Delta = 3$ percent, the $k_i - \omega$ curves yield only single peaks. This can be explained by the

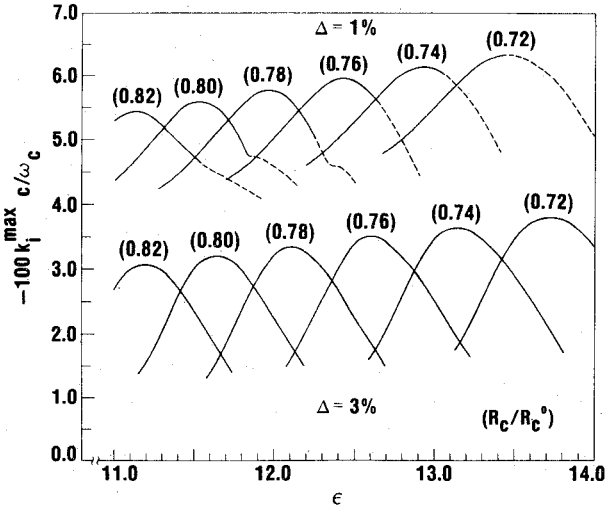

Fig. 4. Plots of the maximum gain ($-k_i^{max}$) versus the dielectric constant (ϵ) for several values of the conducting wall radius (R_c), and at two different axial velocity spreads (Δ). For $\Delta = 1$ percent, the gain exhibits double maxima at high ϵ denoted by broken lines.

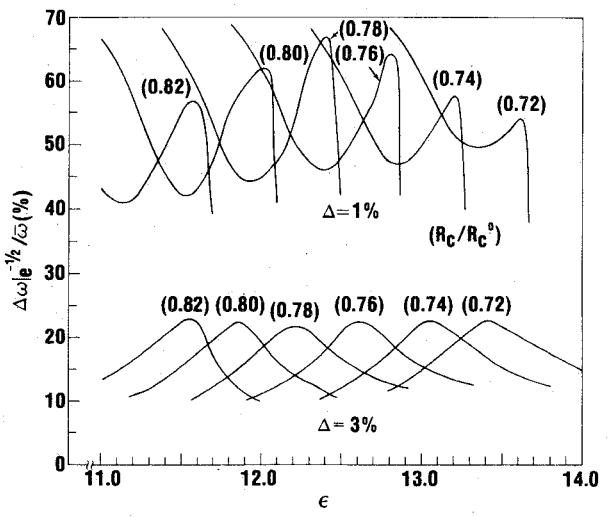

Fig. 5. Plots of the bandwidth ($\Delta\omega$) versus the dielectric constant (ϵ) for several values of the conducting wall location (R_c), and two different velocity spreads (Δ).

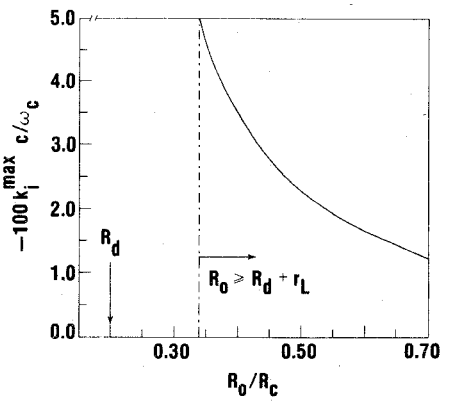

Fig. 6. Dependence of the maximum gain ($-k_i^{max}$) on the beam center location (R_0). The broken vertical line corresponds to the physical lower limit of R_0, where the inner edge of the beam touches the dielectric rod.

greater reduction rate of the gain at higher frequencies for a large spread [2], [4], [6]. That is, the peak at higher frequency is quenched more rapidly when the spread is large. The actual bandwidth for the same parameter in Fig. 4 is shown in Fig. 5. The bandwidth is defined by the full width of the real frequency, at which the linear gain drops to $\exp(-1/2)$ of its maximum value. Of course, the bandwidth is normalized by its mean frequency $\bar{\omega}$. This definition of the bandwidth is somewhat unconventional, but it serves the comparison purposes. For a small spread ($\Delta = 1$ percent), the bandwidth curve in Fig. 5 yields interesting results. For a given wall radius (R_c), as the dielectric constant (ϵ) is increased, the bandwidth decreases, and then increases to give a local peak, followed by an abrupt decrease. Although the bandwidth can be much wider for ϵ lower than that giving local maximum, we attribute this wider bandwidth mainly to the SWM contribution. This is evident from the bandwidth curve for $\Delta = 3$ percent. At ϵ lower than that giving local maxima for $\Delta = 1$ percent, the bandwidth is actually narrower for $\Delta = 3$ percent. In view of the more sensitive nature of the SWM to the velocity spread compared to that of the IWM, we therefore conclude that the wider bandwidth for low ϵ at $\Delta = 1$ percent is due to the SWM. Since our optimization is for the IWM only (suppressing the SWM), the optimized bandwidth of the desired IWM at $\Delta = 1$ percent corresponds to the local maximum. The comparison of Fig. 5 with Fig. 4 reveals that the maximum bandwidth curve (Fig. 5) lies above the maximum gain curve (Fig. 4) as expected from Fig. 2. The optimized values of the dielectric constant and the wall radius are thus given by (from Fig. 5) $\epsilon = 12.6$ and $R_c/R_c^0 = 0.77$. These parameters are to be compared to $\epsilon = 15.2$ and $R_c/R_c^0 = 0.63$ for the wall clad configuration.

The dependence of the gain (and the bandwidth) on the beam center location (R_0) is illustrated in Fig. 6. Here the maximum gain is plotted against the beam location R_0. The physical lower limit of the beam location is depicted by a dotted vertical line in the figure. The maximum gain monotonically decreases as the beam location R_0 is increased. This dependency of the gain is expected, since the instability driving electric field tends to concentrate inside the dielectric center rod. Thus, as the beam is located as close as possible to the edge of the center rod, the gain is increased. At the same time, the SWM is also enhanced by locating the beam as close as to the axis of symmetry ($z = 0$) [2], [4], [6]. This similar behavior of the gain for the SWM and IWM with respect to the beam location is in contrast to that for the wall clad case. There, since the dielectric is attached to the outer conductor, the IWM gain is increased as R_0 increases. On the other hand, the SWM gain is increased as R_0 reduces regardless of the dielectric location [2], [4], [6]. This cooperative nature of the IWM and SWM in the center rod geometry results in the extended IWM region in the frequency space as shown later. The optimized beam location is then given by $R_0 \simeq R_d + r_L$. The results of Figs. 4 and 5 are obtained at this optimized beam location.

The process of the bandwidth optimization is further

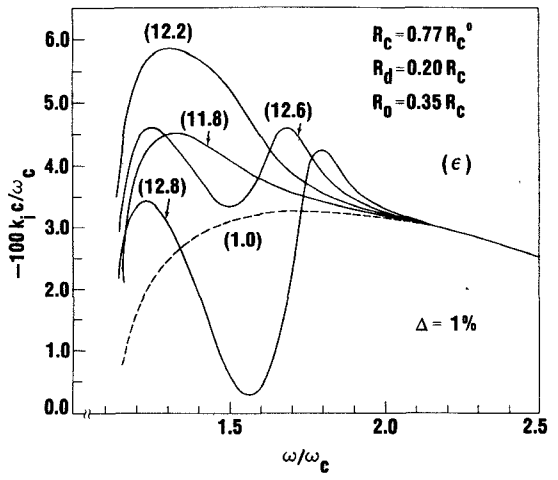

Fig. 7. Plots of the gain ($-k_i$) versus the frequency (ω) for several values of the dielectric constant (ϵ). Other optimized parameters are as shown. The broken line ($\epsilon = 1.0$) corresponds to the absence of the dielectric rod.

illustrated in Fig. 7. Here the gain is plotted versus the frequency for $\Delta = 1$ percent and several values of the dielectric constant. The other parameters are optimized as shown. As a reference, the case for $\epsilon = 1$, that is without the dielectric, is also shown (broken curve). The maximum gain is achieved at the single peak for $\epsilon = 12.2$, corresponding to a point in the maximum gain curve in Fig. 2 (case *B*). For lower ϵ ($\epsilon = 11.8$) the gain yields a single peak at a lower gain, corresponding to case *A* in Fig. 2. For higher ϵ ($\epsilon = 12.6, 12.8$), the beam mode intersects the waveguide mode at two frequencies (case *C* in Fig. 2), resulting in double maxima at those frequencies. As ϵ increases from its maximum gain value ($\epsilon = 12.2$), the gains at the peaks as well as the gain at the valley decrease. Therefore, as ϵ increases from $\epsilon = 12.2$, the bandwidth, now utilizing both peaks, increases until its maximum is reached at $\epsilon = 12.6$. After the maximum bandwidth, the gain at the valley is too low for the bandwidth to include both peaks (e.g., $\epsilon = 12.8$). This explains why the bandwidth in Fig. 5 decreases abruptly after the maximum value. Fig. 7 also provides information on the contribution of the SWM. Since the gain for $\epsilon = 1$ (without the dielectric, broken line) represents the contribution of the SWM only, we can say that any significant difference from this curve is due to the IWM. We note from Fig. 7 that the significant SWM contribution is for the frequency $\omega/\omega_c \gtrsim 2.0$. This is to be compared with $\omega/\omega_c \gtrsim 1.8$ for the pure IWM and $\omega/\omega_c \gtrsim 1.6$ for the mixed mode operation in the wall clad configuration [6, figs. 3, 4(a)], [9]. (With the wall clad configuration, the pure IWM operation is achieved with the beam location close to the wall clad dielectric, and the mixed mode operation with the beam close to the axis [6].) That is, the SWM begins to contribute significantly to the bandwidth at considerably higher frequency with the center rod configuration than with the wall clad configuration, thereby enhancing the frequency range of the IWM for the center rod configuration. In view of the difficulties associated with the SWM, therefore, the center rod configuration is superior to the wall clad geometry.

The foregoing optimization process with respect to the bandwidth, for 1 percent of the axial velocity spread and the beam parameters given in (9), can be summarized as follows:

$$R_d/R_c = 0.20, \quad \epsilon = 12.6, \quad R_c/R_c^0 = 0.77,$$
$$R_0 = R_d + r_L = 0.35\, R_c. \tag{11}$$

The optimized bandwidth at $\Delta = 1$ percent is 68 percent (Fig. 7), of which 51 percent is due to the IWM, and 17 percent to the SWM. This proportion is obtained from Fig. 7, attributing the portion for $\omega/\omega_c \geq 2.0$ to the SWM. This bandwidth can be compared to 46 percent (all IWM) for the pure IWM and 90 percent (12 percent IWM+78 percent SWM) for the mixed mode with the wall clad configuration [6]. Moreover, the mean frequency $\bar{\omega}$ for the center rod gyrotron is $\bar{\omega}/\omega_c = 1.72$, higher than 1.53 for the pure IWM and less than 2.04 for the mixed mode with the wall clad geometry [6]. If we assume that the entire SWM contribution is nonusable, then the bandwidth of the center rod gyrotron is slightly wider than that of the pure IWM and much wider than that of the mixed mode of the wall clad gyrotron.

IV. Perturbed Fields

In the previous section we have seen that the frequency range of the IWM for the center rod configuration is wider than that for the wall clad geometry. Since the IWM results from the beam-waveguide mode coupling, its perturbed field profile is very similar to that of the beam-free waveguide, that is, of Bessel function type. On the other hand, the field profile due to the SWM is highly localized near the beam location [2], [4], [6]. Therefore, we can determine the nature of the instability by plotting the field profiles. The instability driving fields $E_{\theta 1}$ and B_{r1} are given in (3) and (4). Since the instability occurs near the beam mode, the field profiles are computed at $k = k_B \equiv (\omega - \omega_c/\gamma)/c\beta_z$ for given ω. The quantity k_B is the wavenumber corresponding to $\omega = \omega_B$ ((8)). Since, the IWM frequency range, $(\omega^2/c^2 - k_B^2) < 0$, the Bessel functions J and N with arguments x's ((7)) now become the modified Bessel functions I and K.

In Fig. 8, the field profiles of $E_{\theta 1}$ and B_{r1} at a particular frequency $\omega = 1.7\ \omega_c$ are shown for several values of the dielectric constant. That is, the profiles are drawn from Fig. 7 at that frequency. The fields are normalized such that $\int_0^{R_c} (\epsilon_j E_1^2 + B_1^2) r\, dr = R_c^2$. Here $\epsilon_j = \epsilon(1)$ for $r < R_d$ ($r > R_d$). The chosen frequency $\omega = 1.7\ \omega_c$ corresponds approximately to the transition point between the IWM and SWM (Fig. 7). We observe in Fig. 8 that the profile for $\epsilon = 1$ (without the dielectric) is highly localized at the beam location (R_0) with a negligible field amplitude in the space ($r < R_d$) where the dielectric rod is supposed to be. This is, of course, expected since the instability for $\epsilon = 1$ is solely due to the SWM. Without the dielectric ($\epsilon = 1$), the waveguide mode is a fast wave ($\omega_G > ck$), and the slow wave IWM is absent. As ϵ increases the SWM contribution is

TABLE I
COMPARISON OF THE BANDWIDTH-OPTIMIZED DIELECTRIC GYROTRON

Dielectric Used As	Center Rod	Wall Clad	
		Pure IWM	Mixed Mode
ϵ	12.6	15.2	
R_c/R_c^0	0.77	0.63	
Thickness Ratio	$R_d/R_c = 0.20$	$R_w/R_c = 0.85$	
Beam Location	$R_0 \geq R_d + r_L$	$R_0 \leq R_c - r_L$	$R_0/R_c = 0.38$
$-100\ k_i^{max}\ c/\omega_c$	4.6	5.6	3.8
Significant SWM Contribution	$\omega/\omega_c \gtrsim 2.0$	$\omega/\omega_c \gtrsim 1.8$	$\omega/\omega_c \gtrsim 1.6$
Mean Frequency	$\bar{\omega}/\omega_c = 1.72$	$\bar{\omega}/\omega_c = 1.53$	$\bar{\omega}/\omega_c = 2.04$
Bandwidth (IWM + SWM)	68% (51 + 17)	46% (46 + 0)	90% (12 + 78)
$-100\ k_i^{max}\ c/\bar{\omega}$	2.7	3.9	1.8

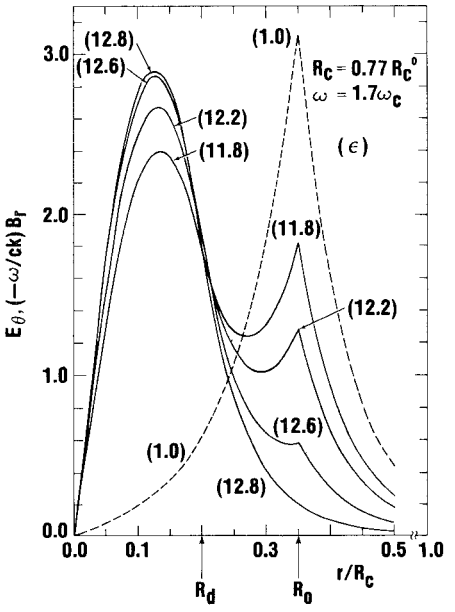

Fig. 8. Perturbed field profiles for several values of the dielectric constant (ϵ) for $\omega/\omega_c = 1.7$ and parameters otherwise identical to those in Fig. 7

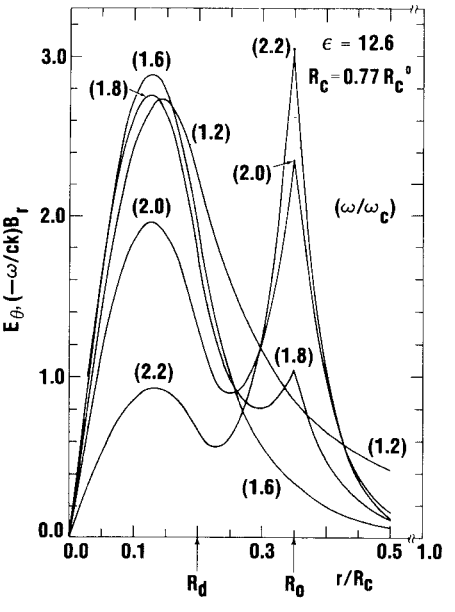

Fig. 9. Perturbed field profiles for several values of the frequency (ω) at the optimized parameters given in (11).

decreased, as indicated by the decreasing peaks of the field profile at the beam location. The reduced SWM contribution with increased ϵ, in turn, indicates the more enhanced IWM contribution (Fig. 2). For example, at $\epsilon = 12.8$, the field profile is almost identical to that of the waveguide, indicating nearly pure IWM contribution to the instability. At $\omega/\omega_c = 1.7$, the significant SWM contribution is for $\epsilon \lesssim 11.8$, as can be confirmed from Fig. 7. In terms of difficulties associated with the microwave excitation and collection, the localization of the field strength due to the SWM at the beam location can be a nuisance. However, these difficulties can be eliminated by optimizing the parameter ϵ, i.e., $\epsilon = 12.6$ in Fig. 8.

The frequency dependence of the field profile is shown in Fig. 9 for the optimized parameters given in (11). As the frequency increases, the peak at the beam location (R_0) is more pronounced. This indicates that the contribution of the SWM is nearly negligible for $\omega/\omega_c \lesssim 1.8$ and is signifi-

cant for $\omega/\omega_c \gtrsim 2.0$, confirming the similar conclusion from Fig. 7. This profile can be compared with that for the mixed mode with the wall clad geometry [6, fig. 6], where the SWM is significant for $\omega/\omega_c \gtrsim 1.6$. We thus again find that the center rod configuration extends the IWM region further than the wall clad gyrotron.

V. Conclusion

We have investigated the wide-band capability of the gyrotron with a dielectric material used as a center rod. After deriving the dispersion relation for the azimuthally symmetric, TE perturbations, we have found the optimization conditions on the physical parameters for a wide bandwidth at a small axial velocity spread ($\Delta = 1$ percent).

The results of the optimization processes and the comparison with the wall clad configuration can be summarized in Table I. All values are obtained with the beam parameters in (9). The center rod configuration allows larger wall dimension, lower dielectric constant, and thicker center rod compared to the wall clad configuration. The gain for the center rod configuration is slightly lower than that of the pure IWM for the wall clad configuration, but higher than that of the mixed mode for the wall clad configuration. The bandwidth is wider than the pure IWM, but narrower than the mixed mode. However, in terms of difficulties associated with the SWM, the center rod configuration proves to be superior in the bandwidth to both the pure IWM and the mixed mode. This advantage comes from the extended IWM frequency range in the center rod configuration.

The optimum beam location, being as close as possible to the dielectric center rod may pose some difficulties in the actual experiment. The dielectric surface effects (e.g., charge build-up, heat dissipation), which are ignored in this paper, must be addressed to. Some compromise in the beam location, therefore, may be essential in the experimental setup. Also, it should be pointed out, the problem of supporting the center rod, and the resulting disturbance in the RF field structure should be considered in the actual device.

References

[1] H. S. Uhm and R. C. Davidson, *Phys. Fluids*, vol. 23, p. 2538, 1980.
[2] J. Y. Choe, H. S. Uhm, and S. Ahn, *J. Appl. Phys.*, vol. 52, p. 4508, 1981.
[3] H. Keren, J. L. Hirschfield, S. Y. Park, K. R. Chu, and J. M. Baird, *Proc. Fifth Int. Conf. Infrared Millimeter Waves*, p. 96, 1980.
[4] J. Y. Choe, H. S. Uhm, and S. Ahn, *IEEE Trans. Nucl. Sci.*, vol. NS-28, p. 2918, 1981.
[5] A. K. Ganguly and K. R. Chu, Naval Research Laboratory, Memo 4215, 1980.
[6] J. Y. Choe, H. S. Uhm, and S. Ahn, *J. Appl. Phys.*, vol. 52, p. 7067, 1981.
[7] H. S. Uhm, J. Y. Choe, and S. Ahn, *Int. J. Electronics*, vol. 51, p. 521, 1981.
[8] J. Y. Choe, H. S. Uhm, and S. Ahn, "Simple description of amplification mechanism in microwave tubes," *Bull. Amer. Phys. Soc.*, vol. 26, p. 908, 1981.
[9] Regardless of the dielectric location, the SWM coexists with the IWM. The pure IWM operation refers to the situation where, through adjustment of the beam location, the contribution of the SWM is negligible in the IWM frequency range (see [6]).

Joon. Y. Choe, photograph and biography not available at the time of publication.

Han S. Uhm, photograph and biography not available at the time of publication.

Saeyoung Ahn (M'77) received the M.A. and Ph.D degrees in physics from Yeshiva University, New York, NY, in 1971 and 1973, respectively, ad te B.S. degree in physics from Seoul National University, Seoul, Korea, after military service in Korea.

Since 1977 he has been a Research Physicist in the Microwave Tube Staff in the Electronics Technology Division, Naval Research Laboratory, Washington, DC. He was a Staff Engineer at Locus, Inc., from 1976 to 1977, and a Visiting Scientist to the Plasma Physics Division and Division of Mathematics and Information Sciences of the Naval Research laboratory from 1974 to 1976. He worked as a Research Associate in the Physics Department, University of Pennsylvania at Philadelphia, PA, from 1974 to 1976, and in the Research Foundation of State University of New York, Albany, NY, from 1972 to 1974. His areas of interst are the millimeter and microwave tubes, the wave-beam interaction, the wave propagation in the inhomogeneous medium, and the remote sensing of subsea surface structure.